Chinese Chemical Letters 34 (2023) 107837

Contents lists available at ScienceDirect

Chinese Chemical Letters

journal homepage: www.elsevier.com/locate/cclet

Efficient degradation of sulfacetamide by CoFe PBAs and PBA@PVDF composite membrane activating peroxymonosulfate

Ruonan Guo[a], Ying Chen[a], Ying Yang[a], Jiangwei Shang[a,b], Xiuwen Cheng[a,b,*]

[a] Key Laboratory for Environmental Pollution Prediction and Control, Gansu Province, College of Earth and Environmental Sciences, Lanzhou University, Lanzhou 730000, China

[b] Key Laboratory of Pollutant Chemistry and Environmental Treatment, College of Chemistry and Environmental Science, Yili Normal University, Yining 835000, China

ARTICLE INFO

Article history:
Received 14 January 2022
Revised 23 August 2022
Accepted 19 September 2022
Available online 23 September 2022

Keywords:
Prussian blue analogues
Peroxymonosulfate
Sulfacetamide
Composite membrane

ABSTRACT

More and more antibiotics that are difficult to biodegrade have been detected in water environments threatening ecosystems and human health. Therefore, it is urgent to develop efficient water treatment methods to degrade antibiotics. In this work, Co-Fe Prussian blue analogues (PBAs) with different molar ratios were synthesized for peroxymonosulfate (PMS) activation to degrade sulfacetamide (SAM, 10 mg/L). By increasing Co molar ratio, the PMS activation capability and electrochemical properties of PBAs were enhanced. Due to its excellent reactivity (degradation efficiency of 84.2% and mineralization efficiency of 52.79%), cost benefit (electrical energy per order, 0.01019 kWh/L) and lower metal leaching ([Co] = 0.259 mg/L, [Fe] = 0.128 mg/L), PBA-1, the as-prepared catalyst with a molar ratio of cobalt to iron of 1:1, was selected for further study. The radical scavenging experiments and an electron paramagnetic resonance (EPR) trapping experiments were performed and revealed that PBA-1 addition was required to produced $^{\bullet}OH$ and $SO_4^{\bullet-}$ from PMS activation. Accordingly, we proposed a PMS activation mechanism and SAM decomposition pathways for PBA-1/PMS reaction system. Besides, a PBA-1@polyvinylidene fluoride (PVDF) catalytic membrane was further prepared to expand the application potential of PBA nanoparticles. The PBA-1@PVDF catalytic membrane was highly effective and exhibited a great reusability; thus, it could be considered for applications in actual water treatment processes.

Pollution caused by increasingly serious antibiotics and their metabolites is one of the most pervasive problems afflicting human and ecosystem health throughout the world, and has drawn the attention of researchers worldwide [1,2]. Sulfonamides (SAs) were first synthesized in 1937 and are the earliest antibiotics that were used in clinical applications. Due to their low cost and broad-spectrum antimicrobial applications, SAs are widely used to treat infection in humans, plants and livestock [3]. More than ten types of SAs have been detected in rivers, sediments, groundwater and soil in many countries, including the United Kingdom, the United States, Australia and China [2,4,5]. The widespread distribution of SAs in aqueous environments can induce the evolution of resistant pathogens, even at lower concentrations, threatening ecosystems and human health [6].

The SAs removal performance of ozonation [7] and advanced oxidation processes (AOPs) involving hydroxyl radicals ($^{\bullet}OH$) [8] has been evaluated. Compared with the abovementioned treatment methods, sulfate radical ($SO_4^{\bullet-}$)-based advanced oxidation processes (SR-AOPs) have the following superiorities: (i) $SO_4^{\bullet-}$ possesses a higher redox potential ($E_o = 2.5–3.1$ V) [9] than $^{\bullet}OH$ ($E_o = 1.9–2.8$ V) [10]. (ii) The half-life of $SO_4^{\bullet-}$ (30–40 μs) is longer than that of $^{\bullet}OH$ (<1 μs), allowing for an excellent mass transfer and contact with the target pollutant in heterogeneous catalysis systems [11]. (iii) The organics oxidation in SR-AOPs is independent of pH, while the removal efficiency of $^{\bullet}OH$-based reaction decreases with increasing pH values [12]. (iv) The SR-AOPs leads to a better mineralization rate than that achieved by $^{\bullet}OH$ [13]. (v) $SO_4^{\bullet-}$ is electrophilic, so it would selectively attack organic molecules and prefer to react with electron-donating groups, including the hydroxyl (–OH), amino ($–NH_2$), and alkoxy (–OR) groups and π electrons present on aromatic molecules [12,14]. Considering energy consumption, catalytic activation by metal and metal oxides is a more efficient technology and exhibits quite excellent per-

* Corresponding author at: Key Laboratory for Environmental Pollution Prediction and Control, Gansu Province, College of Earth and Environmental Sciences, Lanzhou University, Lanzhou 730000, China.
E-mail address: chengxw@lzu.edu.cn (X. Cheng).

https://doi.org/10.1016/j.cclet.2022.107837
1001-8417/

formance for pollutant removal [15]. Therefore, we attempted to synthesize transition metal catalyst for SR-AOPs and used sulfacetamide (SAM) as a target pollutant.

Prussian blue (PB) has a unique internal chemically tunable feature, in which the Fe metal centers can be replaced by different metal ions (such as Co, Ni, Zn) to produce electrochemically active analogs (PBAs). PBAs are well known porous coordination polymers (PCPs) with a chemical formula of $M_n[\acute{M}_m(CN)_6]\cdot xH_2O$ (where M and Ḿ represent transition metal cations). PBAs have definite compositions of metal cations, which act as nodes that are linked by cyanide groups which act as bridges [16]. Therefore, due to the unique internal chemically tunable feature of PBAs, we believe that peroxymonosulfate (PMS) activation using PBAs is easier to maintain, overcoming the drawback of poor stability of supported catalysts. More importantly, the robust framework of PBAs exhibits a great stability which reduces secondary contamination by toxic metal-leaching in strong acid/basic conditions as compared with traditional transition metal catalysts [17,18]. Zeng *et al.* [19] synthesized PBAs@poly(*m*-phenylenediamine) nanoparticles with core-shell structure to activate PMS for degradation of Rhodamine B (RhB). Interestingly, the Co leaching concentration was reduced after coating a layer of PmPD on the surface of Fe-Co-Co PBA. Wu *et al.* [20] prepared Fe/Mn PBA@PBAs catalysts with core-shell structure and exhibited excellent pollutant removal performance. Zhang *et al.* [21] confirmed that Fe/Co PBAs have a high activity to activate PMS and high-efficiency degradation of bisphenol A, meanwhile, Fe shell in this heterogeneous catalyst can effectively protect and inhibit the leaching of cobalt ions. Nevertheless, previous studies on the PBAs-based persulfate catalysts were usually prepared by complex and cumbersome procedures. Thus, developing a facile method to synthesize PBAs with great catalytic capability remains a top priority and highly desirable.

Furthermore, the stability and recyclability of nanocatalysts is important, but most researchers have neglected the separation of nanomaterials from treated water, which can cause secondary pollution [22–24]. According to previous review, PBAs loaded in solid supporters enrich themselves with versatile forms and better mechanical strength [25]. Due to their good film forming properties, toughness and separation properties, polymer substrates have become one of research hotspots in the immobilization catalyst field. In particular, polyvinylidene fluoride (PVDF) has received extensive attention for wastewater purification applications because of its excellent chemical resistance, thermal stability and high mechanical strength [26]. In this study, we developed an economical and effective PBA nanoparticle-loaded catalytic membrane to achieve PMS activation, which simultaneously oxidized organic pollutants and efficiently recovered the catalyst.

In this study, CoFe PBAs were prepared and used to activate PMS. And the organic pollutant oxidation potential, reusability and optimal reactive conditions of PBA/PMS reaction system were evaluated. In the course of experimental inquiry, SAM was selected as the target compound and its decomposition pathways were proposed. Besides, electrochemical detection methods and X-ray photoelectron spectroscopy (XPS) measurements were applied to explain the mechanism of the excellent PMS activation performance of the PBAs. Lastly, a PBA-1@PVDF catalytic membrane, which could be separated from water expediently overcoming the problem of catalyst recycling, was further prepared to expand the application potential of PBA nanoparticles.

A co-precipitation strategy was used to synthesize the CoFe PBAs. First, a certain amount of 0.01 mol $K_3[Fe(CN)_6]$, 0.01 mol $Co(NO_3)_2\cdot 6H_2O$ and 3.000 g polyvinyl pyrrolidone (PVP) solid powder were added into 200 mL deionized water. After all the reagents were fully dissolved, the suspension was then aged at 30 °C for 30 min with constant stirring. After aging, the solid material was washed by deionized water and ethanol with the assistance of a centrifugation treatment and dried at 60 °C for 48 h. The processes used to prepare PBA-0.5, PBA-2, PBA-3 and PBA-4 various ratios of $K_3[Fe(CN)_6]$ and $Co(NO_3)_2\cdot 6H_2O$ (*i.e.*, 1:2, 2:1, 3:1 and 4:1, respectively).

As optimized PBA-1 was used to prepare the PBA-1@PVDF (with PBA-1 mass ratio as 1.6%) composite membranes and the details are presented here. First, 4.000 g PVDF particles were dissolved into 16.0 mL of DMAC at a temperature of 80 °C and the solution was stirred. After the PVDF particles were fully dissolved, a gelatinous solution was formed. Then, 0.320 g of $(NaPO_3)_6$, 0.800 g of PVP and 65 mg PBA-1 nanoparticles were slowly added into the PVDF solution. Next, after standing overnight to remove bubbles, the colloidal mixture was poured onto a glass plate (10×10 cm^2) and scraped to prepare the flat PBA-1@PVDF composite membranes (about 2.6 g, 10×10 cm^2). Note that the as-obtained PBA-1@PVDF membranes were stored in glass bottles filled with ethanol and deionized water (with a volume ratio 1:1).

In this study, SAM was selected and served as probing molecule to evaluate the PMS activation performance of PBAs. All the activation performance experiments were carried out at 30 °C with initial pH 5.85 of SAM aqueous solution (10.0 mg/L). For reaction system, 6.0 mg PBA-1 was dispersed into 100 mL SAM solution. And then, 30.0 mg PMS would be added. At given time intervals, about 3 mL treated sample was taken and filtered with 0.22 μm nitrocellulose membrane to detect the concentration of SAM *via* ultraviolet spectrophotometer. Moreover, the PMS activation performance of PBA-0.5, PBA-2, PBA-3 and PBA-4 were determined as reference. With respect to PBA-1@PVDF composite membrane system, 100 mL SAM solution (10.0 mg/L) would be treated by 30.0 mg PMS and PBA-1@PVDF membrane (5×10 cm^2, about 0.264 g). At given time intervals, about 3 mL treated simulated pollutant solution would be collected and detected by ultraviolet spectrophotometer to confirm remained SAM concentration. Furthermore, to identify intermediate products, samples were analyzed using high-performance liquid chromatography tandem mass spectrometry (HPLC-MS) measurement including Waters HPLC (2010, USA) coupled with a triple-stage quadrupole mass spectrometer (Thermo Scientific TSQ Quantum Access MAX, USA) *via* positive-mode electrospray ionization (ESI^+). Separation was conducted by a C18 HPLC capillary column (100 mm × 2.1 mm i.d., 5 μm, Thermo, USA). A mixed solution of acetonitrile and deionized water (v/v, 55%/45%) was selected as mobile phase A. Besides, 0.1% formic acid and 5×10^{-3} mol/L ammonium formate water solution was used as mobile phase B. The flow rate of mobile phases, injection volume of the sample, and excitation wavelength were maintained at 1 mL/min, 20 μL and 264 nm, respectively.

In order to obtain optimized conditions, the effects of key parameters, concluding PBA-1 dosage, PMS concentration, pH value, reaction temperature, humic acid and different anions were studied. Adjusting the pH value of the reaction system *via* 1 mol/L KOH and 1 mol/L H_2SO_4. Diverse anions, *i.e.*, Cl^-, NO_3^- and HCO_3^-, were induced through KCl, KNO_3 and $KHCO_3$, respectively. The heterogeneous catalyst activation of PMS produces various reactive radicals, such as sulfate radicals ($SO_4^{\bullet-}$), hydroxyl radicals ($^{\bullet}OH$) and superoxide radicals ($^{\bullet}O_2^-$) [27]. It was essential to determine the role of these radicals in order to deduce the SAM oxidation pathways and reaction mechanism. Ethanol was applied as the scavenger of $^{\bullet}OH$ (9.1×10^6 L mol^{-1} s^{-1}) as well as $SO_4^{\bullet-}$ (3.5×10^7 L mol^{-1} s^{-1}) [28]. Besides, *tert*-butyl alcohol (TBA) was selected to identify $^{\bullet}OH$ ($(3.8\text{-}7.6) \times 10^8$) [29]. Moreover, it was commonly accepted that *p*-benzoquinone (BQ) acted as quenching agent for $^{\bullet}O_2^-$ [30]. In recycling experiment, the used catalyst in suspension was gathered by centrifugal separation. Next, it would be washed by ethanol and deionized water, and then dried overnight in oven at 60 °C for further use. As for used PBA-1@PVDF membrane, it was collected *via* tweezers, then, washed and stored

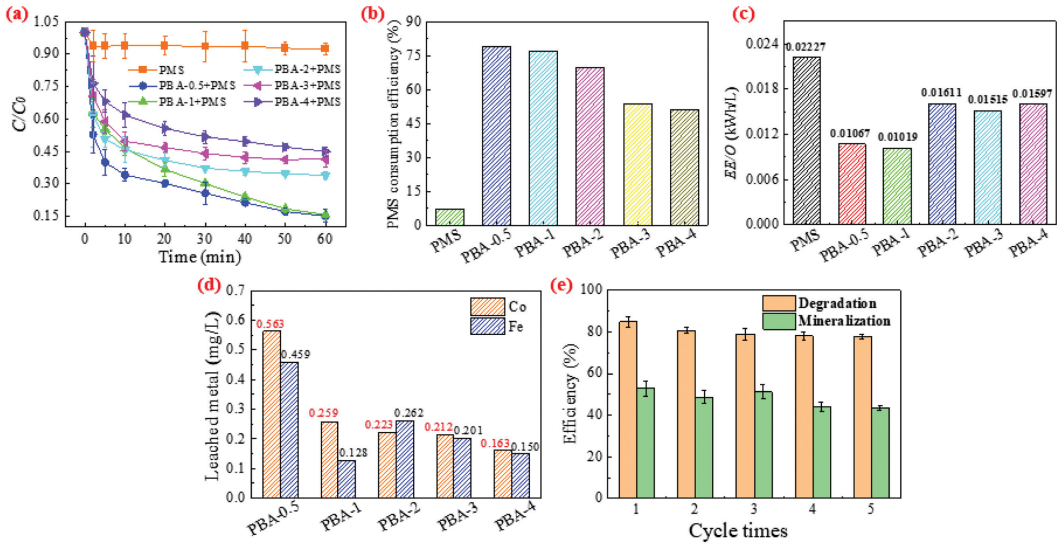

Fig. 1. (a) Removal efficiency of SAM, (b) corresponding PMS consumption efficiency, (c) EE/O values and (d) metal ions leaching amount (reaction conditions: $[Catalyst]_0 = 60$ mg/L, $[PMS]_0 = 300$ mg/L, $[SAM]_0 = 10$ mg/L, pH 5.85 (unadjusted), reaction temperature = 30 °C). (e) PBA-1/PMS reaction system SAM removal efficiency used to determine the repeatability (reaction conditions: $[PBA\text{-}1]_0 = 60$ mg/L, $[PMS]_0 = 300$ mg/L, $[SAM]_0 = 10$ mg/L, pH 5.85 (unadjusted), reaction time = 60 min, reaction temperature = 30 °C).

with ethanol and deionized water (volume ratio = 1) for the next cycle.

Moreover, some characterization analyses were applied to prove repeatability of PBA-1 nanoparticles and PBA-1@PVDF membrane. Besides, chemical characterization methods and electrochemical property detection of PBAs were described in the Text S1 (Supporting information).

To optimize the catalytic performance of PBAs, the impact of different molar ratios of CoFe PBAs on SAM degradation was investigated and displayed in Fig. 1a. By increasing the Fe molar ratio, the SAM degradation efficiency reduced to 84.8%, 84.2%, 66.0%, 58.6% and 55.0% after 60 min. Meanwhile, as displayed in Fig. 1b, the PMS consumption efficiency was confirmed. Fig. 1c shows the electrical energy per order (EE/O) for SAM (The EE/O values for SAM removal were calculated and the methodology is described in Text S2 in Supporting information) [31,32]. As a result, the EE/O value of the PBAs/PMS decreased significantly as compare to that of PMS alone, and this reveals the benefit of adding PBA. Nevertheless, the EE/O value of PBA-1/PMS was 0.01019 kWh/L, which was the lowest EE/O for the various catalysts reaction systems in this study (Fig. 1c). Fig. 1d and Fig. S2 (Supporting information) showed the change in the leached metal amount and percentage with different PBAs after 60 min of the reaction. Clearly, PBA-1/PMS system simultaneously exhibited a great SAM degradation and a significant decrease in the Co and Fe leaching as compared to PBA-0.5. As depicted, all the cobalt ion leaching concentrations of as-obtained PBAs were lower than the limited cobalt ion concentration (1.0 mg/L) in the Environmental Quality Standards for Surface Water (GB3838-2002) of China. Nevertheless, the iron ion leaching concentrations of PBA-0.5 exceeded the limited concentration (0.3 mg/L) in the national standard (GB3838-2002), and the dissolved iron ion concentrations of another PBAs were lower than the standard limit concentration. For metal-based catalysts, the secondary pollution issue caused by the leached metal ions is of great concern. In particular, the cobalt ions released into environments are possibly toxic and carcinogenic. Considering the EE/O value and Co^{2+} dissolution, PBA-1 was selected for further study. Additionally, the stability and reusability of PBA-1 were evaluated by SAM removal efficiency (Fig. 1e) and characterization (Figs. S3-S5 in Supporting information) as discussed in Text S3 (Supporting information).

The microscopic morphologies of the PBAs with different molar ratios of Co and Fe were depicted in Fig. 2 and Fig. S6 (Supporting information). It was clearly that with different Co and Fe amount, the morphology would change. These as-obtained PBAs sample were in agglomerated state under low magnification condition (× 1.0k). Particularly, the surface of PBA-1 sample (Fig. 2a) was smoother than another PBA-0.5 (Fig. S6A-1). Seen from Fig. S6A-1-D-1, with the increasing molar ratio of Fe, the surface of the particles was getting rougher. Nevertheless, with higher magnification (× 10.0k), it would be seen that morphology of PBAs (Fig. 2b and Figs. S6A-2-D-2) was bumpy particles agglomerate with different postures. For instance, compared with PBA-1 (Fig. 2b), the particle structure of PBA-0.5 (Fig. S6A-2) surface was more difficult to observe, which may be favorable to stability of catalyst. Whereas, PBA-1 had more channels on the surface based on tightly bonded particle structure, which was further determined *via* TEM images (Figs. 2d and e). The special microscopic structure would induce more reactive site in PBA-1. Moreover, the detailed microscopic morphologies of PBAs were obtained under higher magnification (× 50.0k). Notably, the above particle agglomerates are composed of nanoparticles. Seen from Fig. 2c and Figs. S6A-3-D-3, the particle structure become firmer with the increase of Fe molar ratio. And the size of nanoparticles which constituted the above-mentioned particles was different in the agglomerate structure of as-prepared PBAs. Fig. 2f and Fig. S6 depicted particle size distribution of PBA-1, PBA-0.5, PBA-2, PBA-3 and PBA-4 samples, indicating that the size of nanoparticles developed. Overall, the PBA-1 possessed more pore structure on the surface and would provide more reactive site to PMS and pollutants, and the tightly bonded particle structure was easier to preserve during the reaction, as shown in Fig. S6.

Surface elements mapping of PBA-1 were shown in Figs. 2g-j, revealing the existence of O, C, Fe and Co. Besides, the EDS spectrum depicted that the experimental molar ratio of Co and Fe were close to designed theoretical stoichiometric value (Fig. 2k).

As shown in Fig. 2l, the XRD patterns of the as-obtained CoFe PBAs show characteristic peaks of Prussian blue analogues with face centered cubic structures ($Co_3[Fe(CN)_6]\cdot 10H_2O$, JCPDS No. 46-0907) [33,34]. The peaks at that were observed at approximately

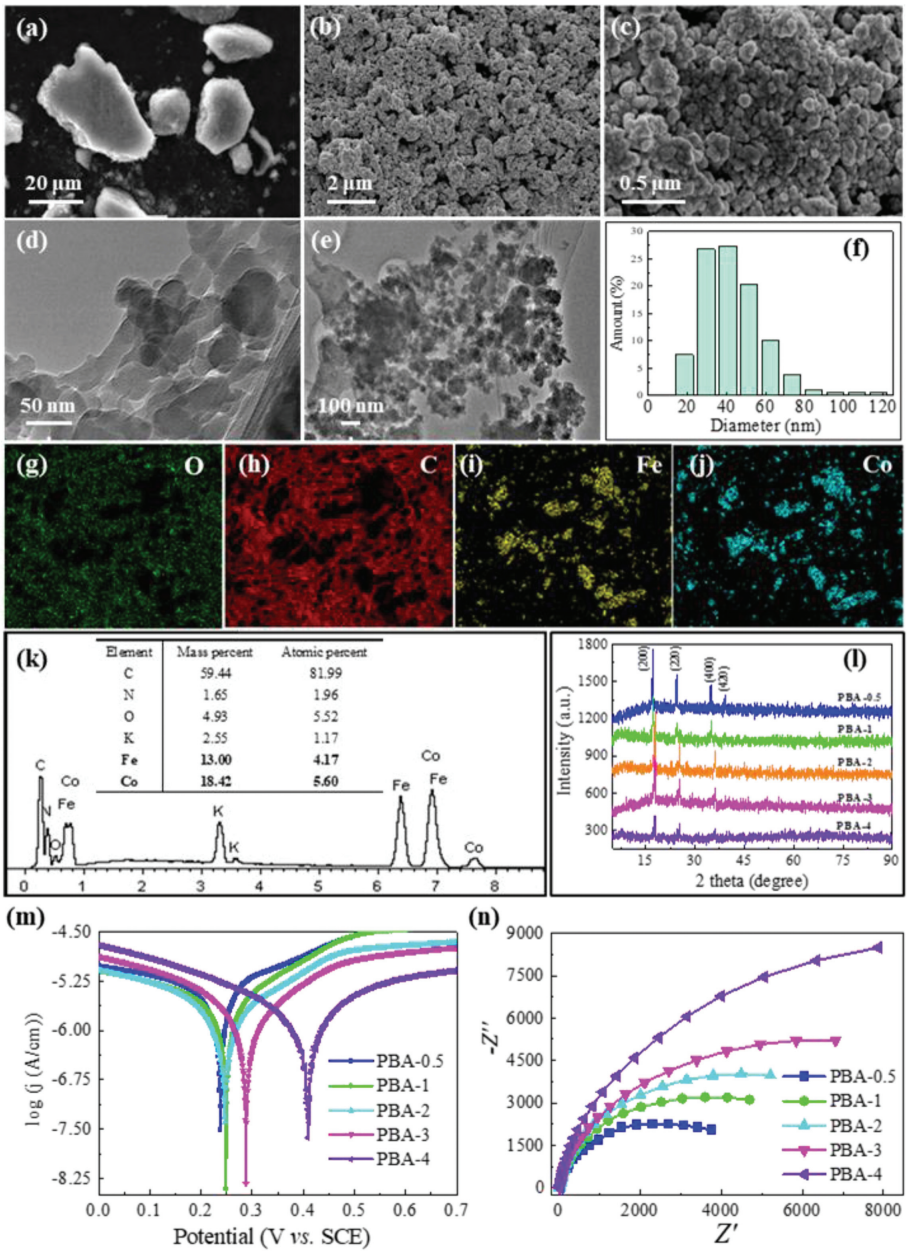

Fig. 2. (a-c) SEM and (d, e) TEM images of the Co_1Fe_1 PBA. (f) Particle size distribution of Co_1Fe_1 PBA. Elemental mapping images of (g) O, (h) C, (i) Fe and (j) Co of the as-obtained Co_1Fe_1 PBA sample. (k) EDS spectrum of the as-obtained Co_1Fe_1 PBA sample. (l) XRD patterns of the as-prepared CoFe PBAs. (m) Tafel polarization curve and (n) electrochemical impedance spectroscopy (EIS) plots of the as-obtained CoFe PBAs.

25° and 35°, are the (220) and (400) planes, and are slightly shifted and broadened. The broadening of the XRD peaks can be related not only to the degree of crystallinity, but also to the crystallite size [35]. The crystallite sizes of the as-obtained PBAs were calculated from Scherrer's formula (Eq. 1).

$$D = K\lambda/\beta\cos\theta \quad (1)$$

where K and λ (*i.e.*, the wavelength of the X-rays) were 0.94 and 0.15418 nm, respectively. β and θ were the half width and half Bragg's angle of the peak. According to Scherrer's formula and the MDI Jade 6.0 software, the crystallite size of PBA-0.5, PBA-1, PBA-2, PBA-3 and PBA-4 were confirmed to be 36.30, 29.55, 37.80, 35.87 and 37.47 nm, respectively.

The electron migration properties influence the pollutant oxidation in the PMS activation process and excellent electron transmission capability of the catalyst is to activating PMS and retaining the catalyst activity [36–38]. In particular, electrons could attack to the peroxide bonds of PMS and produce radical/nonradical reactive species that are capable of SAM oxidation [39,40]. Furthermore, the electrochemical performance is related to the catalyst stability. We measured the electrochemical performance *via* Tafel polarization curves and electrochemical impedance spectroscopy (EIS). According to the Tafel polarization curves (Fig. 2m) obtained for the PBA-0.5, PBA-1, PBA-2, PBA-3 and PBA-4, the corrosion current values were calculated by the CHI660E electrochemical workstation to be 9.637×10^{-6}, 3.689×10^{-6}, 2.209×10^{-6}, 1.438×10^{-6} and 2.060×10^{-6} A, respectively. It was clear that PBA-1 and PBA-0.5 exhibited a much higher corrosion current then the other catalysts, indicating that PBA-1 and PBA-0.5 were with lower charge transfer resistance and had higher electron transfer rate [41]. Nevertheless, with respect to Co^{2+} release, PBA-1, which was with excellent electron transfer performance and catalytic capability, pos-

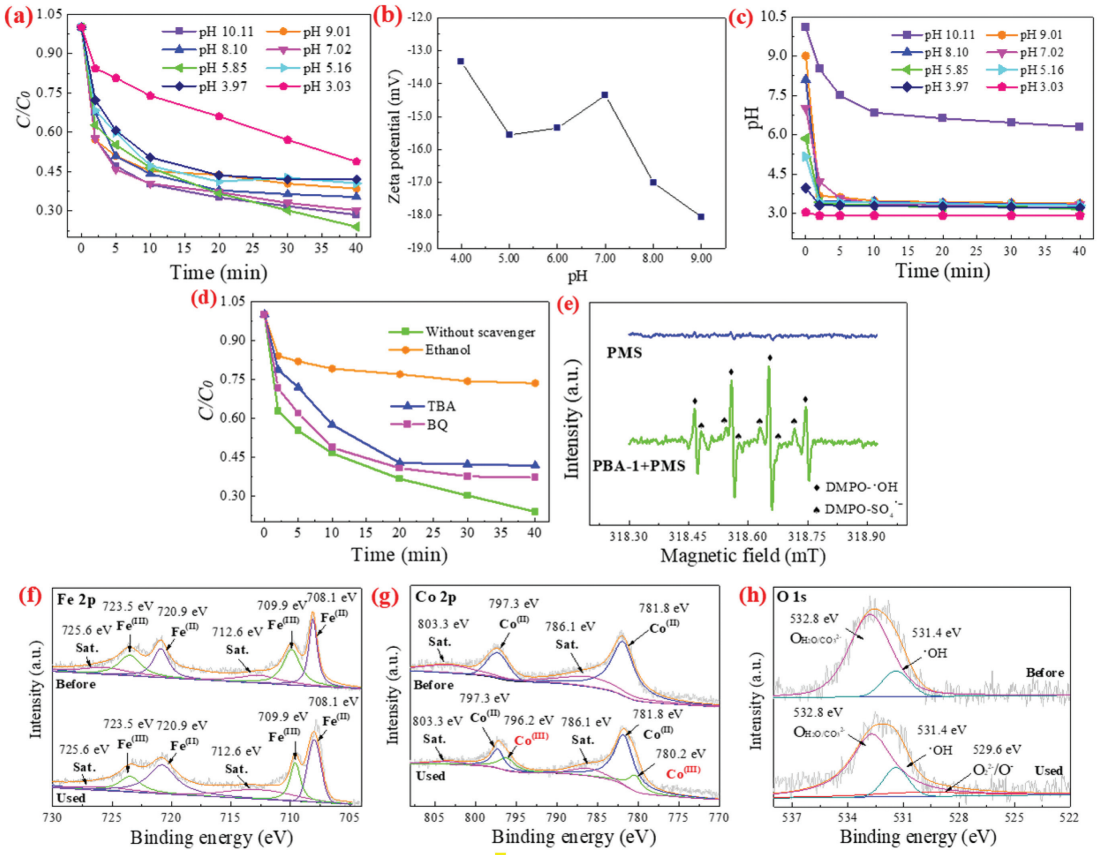

Fig. 3. (a) Effect of pH on the degradation of SAM and (b) pH change (reaction conditions: $[PBA\text{-}1]_0 = 60$ mg/L, $[PMS]_0 = 300$ mg/L, $[SAM]_0 = 10$ mg/L, pH 3.03, 3.97, 5.16, 5.85, 7.02, 8.10, 9.01 and 10.11, reaction temperature = 30 °C). (c) Zeta potential of PBA-1 under different pH values. (d) Effect of the radical scavengers on SAM degradation in the PBA-1/PMS reaction system (reaction conditions: $[PBA\text{-}1]_0 = 60$ mg/L, $[PMS]_0 = 300$ mg/L, [Corresponding radical scavenger] = 10 mmol/L, $[SAM]_0 = 10$ mg/L, pH 5.85 (unadjusted), reaction temperature = 30 °C). (e) EPR spectra in various reactions (reaction conditions: $[PBA\text{-}1]_0 = 60$ mg/L, $[PMS]_0 = 300$ mg/L, reaction temperature = 30 °C, SAM was not added). (f) Fe 2p, (g) Co 2p and (h) O 1s XPS spectra of PBA-1 before and after five cycles of the SAM degradation reaction.

sessed more application potential than PBA-0.5. As shown in Fig. 2n, as the Fe molar ratio increases, a larger arc radius would form, meaning that the resistance to electron transfer would increase. Clearly, PBA-1 possessed an excellent electron transport property, which resulted from an accelerated transfer rate and decreased electrochemical impedance of electrons. Furtherment the improved electrochemical property supported excellent PMS activation performance of PBA-1.

We determined the influence these key reaction parameters: (1) the catalyst dose, (2) PMS concentration, (3) initial pH, (4) temperature and (5) the presence of background substances (*i.e.*, humic acid, Cl^-, NO_3^- and HCO_3^-).

Previous studies have shown that the initial pH played an important role in the oxidation of pollutants [42,43]. We examined PMS activation by PBA-1 for acidic (pH 3.03 and 3.97), weakly acidic (pH 5.16), unadjusted (pH 5.85), neutral (pH 7.02), weakly alkaline (pH 8.10 and 9.01) and alkaline (pH 10.11) pH conditions. As show in Fig. 3a, the oxidation of SAM after a 40 min reaction was 51.2%, 58.0%, 59.5%, 76.1%, 69.8%, 64.7%, 61.5% and 71.5%, respectively. It was obvious that the higher efficiencies (*i.e.*, 76.1, 69.8 and 71.5%) were achieved at pH values of 5.85, 7.02 and 10.11. We analyzed the experimental results as following:

(i) The form of SAM which was with a high reactivity toward oxidants would increase removal performance at pH values of 5.85 and 7.02. In detail, SAM is a typical sulfonamide with a molecular structure similar to that of sulfamethazine. The amine group on SAM is protonated under acidic conditions and transformed into an anion under weakly acidic conditions when the sulfonamide NH group is deprotonated [42]. Moreover, the difference between pH and catalyst pH_{pzc} have influence in wastewater treatment. As depicted in Fig. 3b, the catalyst pH_{pzc} is below than zero and similar to each other, which favors the generation of a negative surface charge on the PBA-1. This negative charge would inhibit the electrostatic interaction between the catalyst surface and PMS species. Nevertheless, under different pH conditions, there was no significant correlation between the degradation trend of SAM and the change rule of pH_{pzc}.

(ii) We had excellent oxidation performance under the alkaline (pH 10.11) conditions and this experimental result is contrary to the results of previous studies [44,45]. To understand how pH impacts the oxidation rate, it should be noted that the ionized species of PMS are affected by pH. HSO_5^- is the dominant species at pH values <9.4, while SO_5^{2-} is the dominant species in strong alkaline solutions ($HSO_5^- \leftrightarrow H^+ + SO_5^{2-}$, $pK_{a2,PMS} = 9.4$). Note that SO_5^{2-} is less reactive than HSO_5^- [46]. As shown in Fig. 3c, we investigated the impact of pH on SAM oxidation. The pH immediately decreased when PMS was added into the solution because the pK_{a1} and pK_{a2} of PMS are 0 and 9.4, respectively [27]. Accordingly, the reaction solution became acidic when the initial pH was lower than 10. When the initial pH was 10.11, the pH dropped to 7.50 after 5 min and was 6.30 after 40 min of reaction and weakly acidic and neutral conditions are more favorable for SAM oxidation.

(iii) Meanwhile, evident decreases in the SAM degradation reaction were observed under acidic (pH 3.03 and 3.97), weakly acidic

(pH 5.16) and weakly alkaline (pH 8.10 and 9.01) conditions. Under acidic conditions (pH < 5), hydrogen ions (H^+) can scavenge for sulfate and hydroxyl radicals, which limits SA removal processes [47]. When the pH increased to more than 7, the man OH^- ions present in the basic solution could activate PMS and efficiently promote SAM degradation [47,48]. Correspondingly, 58.0% and 59.5% of SAM was removed at pH values of 3.97 and 5.16, respectively, and in the meantime, 64.7% and 61.5% of SAMs were destroyed at pH values of 8.10 and 9.01. Therefore, less SAM could be degraded under weakly acidic conditions than under weakly alkaline reaction conditions. However, the pH change was independent of the initial pH of the solution. In contrast to the system at a pH of 10.11, the pH values of another system changed to approximately 3 after a 40 min reaction. When the initial pH was fixed at 3.03, the pH became 2.91 after 2 min, and the SAM degradation efficiency was 51.2% after 40 min. Based on the change in the pH, the SAM degradation reaction efficiency was limited under acidic (pH 3.03 and 3.97), weakly acidic (pH 5.16) and weakly alkaline (pH 8.10 and 9.01) conditions, which differed from the reaction efficiency observed at a pH 5.85, 7.02 and 10.11.

The abovementioned results and discussion illustrated that the PBA-1/PMS reaction system was tolerant to a wide pH range (pH 3.30-10.11). Particularly, the PBA-1/PMS reaction system performed better in slightly acidic and neutral solutions. Most of the natural water had a pH value of 5-9, and thus, the PBA-1/PMS reaction system was suitable for practical wastewater treatment processes [42].

Besides, the detailed analysis of the catalyst dose, PMS concentration, and temperature were introduced in Text S4 (Supporting information). As depicted in Fig. S7 (Supporting information), it was found that PBA-1/PMS reaction system would be influenced with co-existing substance. Results showed that the influence of humic acid and selected three anions on SAM degradation was different. The detailed discussion was listed in Text S4 (Supporting information).

The primary identification of the species was performed using different radical scavengers. As shown in Fig. 3d, the inhibiting effect of ethanol was much higher than that of TBA, which achieved SAM removal efficiency of 26.5% and 58.3%, respectively. This fact proved that both of $^{\bullet}OH$ and $SO_4^{\bullet-}$ played important roles in PBA-1/PMS reaction system, particularly, the involvement of $SO_4^{\bullet-}$ was dominant. To further verify $^{\bullet}OH$ and $SO_4^{\bullet-}$ generation during the PMS activation process, EPR measurement was carried out. Fig. 3e shown EPR spectra of PMS in the presence of DMPO which served as the free radical spin trapping agent. Clearly, there was no noticeable signal when PMS existed in water alone, indicating no formation of DMPO-adducts. However, when PBA-1 was added, signals of DMPO-$^{\bullet}OH$ and DMPO-$SO_4^{\bullet-}$ was detected, that is, $^{\bullet}OH$ and $SO_4^{\bullet-}$ were produced in PMS activation with catalysts addition. Moreover, the function of $^{\bullet}O_2^-$ was determined, which could be identified *via p*-benzoquinone (BQ). Seen from Fig. 3d, with addition of BQ, SAM degradation efficiency reduced from 76.1% to 62.9%, implying that $^{\bullet}O_2^-$ took part in SAM destroy process, whereas, did not act as major reactive oxide factors.

To further study the degradation mechanism of SAM in the PBA-1/PMS reaction system, the intermediate products were detected. All of the transformation products, formulas, *m/z* values and proposed structures are listed in Table S1 (Supporting information). By referring to the nitrogen rule and the analytical approaches described in previous studies, reasonable pathways (I, II and III) of SAM in the PBA-1/PMS reaction system are depicted in Fig. S12 (Supporting information) and discussed in Text S5 (Supporting information).

The XPS spectrum showed that new peaks did not appear, proving the excellent stability of PBA-1 during the PMS activation process. Fig. 3f shows the high-resolution Fe 2p spectra and the Fe $2p_{3/2}$ and Fe $2p_{1/2}$ peaks, which were centered at 708.1 eV and 720.9 eV, respectively, and demonstrated the existence of Fe^{II} in form of $[Fe^{II}(CN)_6]^{2-}$. The peaks at 709.9 eV and 723.5 eV were ascribed to Fe^{III} of $[Fe^{III}(CN)_6]^{4-}$ in the PBA framework. In addition, the two satellite peaks centered at 712.6 eV and 725.6 eV indicated the presence of Fe^{III} [49,50]. It could be observed from the Fe 2p spectrum of the used sample that the binding energy values slightly shifted after the oxidation reaction. In contrast, the total area of the peaks slightly decreased, implying that oxidation occurred during the catalytic process. According to the areas of the two characteristic binding energy peaks, the contents of Fe^{III} and Fe^{II} in the PBA-1 sample before the PMS activation process were 60.75% and 39.25%, respectively. Similarly, the contents of Fe^{III} and Fe^{II} in the PBA-1 sample after the five cycles of the reaction were 67.73% and 32.27%, respectively. According to previous studies, the redox couple between Fe^{II} and Fe^{III} did occur, thus assuring the catalytic capability of PBA-1 (Eqs. 2–4). The intrinsic and generated Fe^{II} would have performance superior to that of PMS for SAM removal [51]. Moreover, $^{\bullet}O_2^-$ is generated during a series of reactions (Eqs. 2–5) [52].

$$FeII + 2HSO_5^- \rightarrow 2^{\bullet}OH + SO4^{\bullet-} + SO_4^{2-} + Fe^{III} \quad (2)$$

$$2^{\bullet}OH \rightarrow H_2O_2 \quad (3)$$

$$Fe^{III} + H_2O_2 \rightarrow Fe^{II} + HO_2^{\bullet} + H^+ \quad (4)$$

$$HO_2^{\bullet} \rightarrow {}^{\bullet}O_2^- + H^+ \quad (5)$$

The high-resolution Co 2p spectrum of PBA-1 before the reaction (Fig. 3g) was well fitted with four contributions, including a pair of spin-orbit doublets and their shakeup satellite peaks, indicating the existence of Co^{II} [53–56]. After repeated SAM degradation experiments, the Co 2p spectrum of PBA-1 depicted little removal; however, two obvious peaks appeared at 796.2 eV and 780.2 eV, which were assigned to the Co $2p_{3/2}$ and Co $2p_{1/2}$ levels, respectively, and illustrated Co^{III} generation. Co^{II} would serve as reactive sites to react with HSO_5^- (Eq. 6), thereby generating abundant $SO_4^{\bullet-}$. Furthermore, the generated Co^{III} would accept electrons from the lattice oxygen of HSO_5^- (Eq. 7) to balance the charge on the PBA-1 surface. In the meantime, many $SO_5^{\bullet-}$ radicals were produced. Because of its much lower reducing potential (1.10 eV), the $SO_5^{\bullet-}$ radical is not responsible for SAM oxidation. As clearly seen from Fig. 3h, two characteristic peaks at 531.4 eV and 532.8 eV could be ascribed to hydroxyl groups ($^{\bullet}OH$) and adsorbed molecular water and carbonates (H_2O/CO_3^-), and meanwhile, the contents of $^{\bullet}OH$ and H_2O/CO_3^- in the PBA-1 sample before the PMS activation process were 14.53% and 85.47%, respectively. The O 1s spectrum obtained for the used sample was deconvoluted into three peaks at 529.9, 531.4 and 532.8 eV, which corresponds to contents of 12.34%, 13.20% and 74.46%, respectively. The new peak at 529.6 eV was assigned to oxygen in the forms of O_2^{2-}/O^- [57]. The decrease in the lattice oxygen content might result from its oxidization to O_2 with the reduction of Co^{III} to Co^{II}, indicating that the adsorbed oxygen was able to form lattice oxygen depending on the oxygen mobility of the oxygen vacancies [57,58]. Hence, $SO_5^{\bullet-}$ would transform to more $SO_4^{\bullet-}$, improving the SAM oxidation efficiency (Eq. 8).

$$Co^{II} + 2HSO_5^- \rightarrow 2^{\bullet}OH + SO_4^{\bullet-} + SO_4^{2-} + Co^{III} \quad (6)$$

$$Co^{III} + 2HSO_5^- \rightarrow SO_5^{\bullet-} + SO_4^{2-} + Co^{II} \quad (7)$$

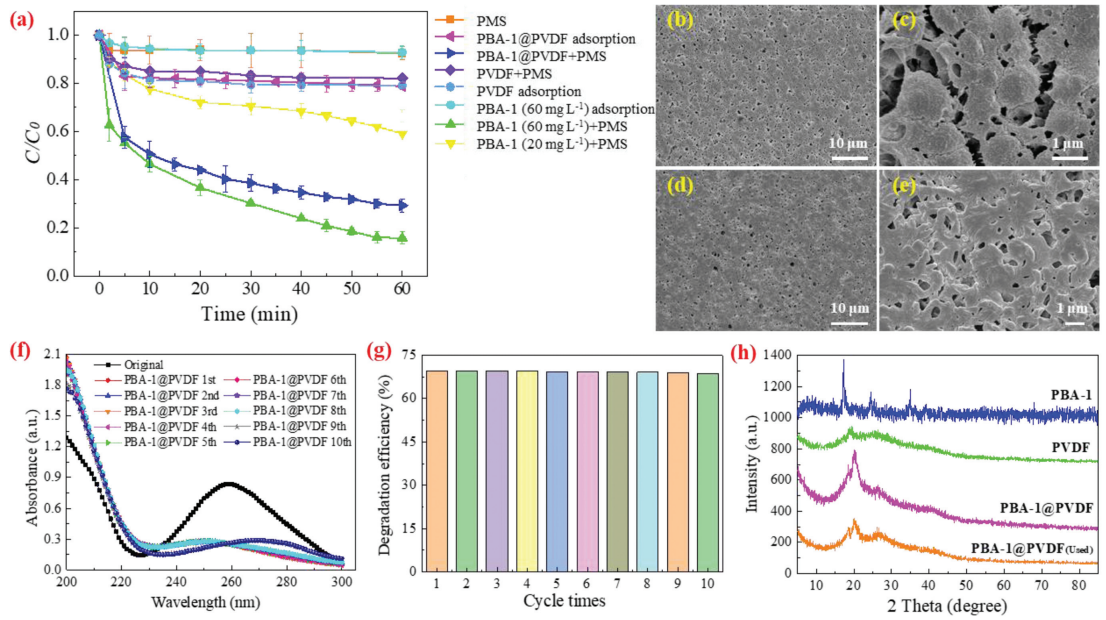

Fig. 4. (a) Removal of SAM in the different reaction systems (reaction conditions: $[PMS]_0 = 300$ mg/L, $[SAM]_0 = 10$ mg/L, pH 5.85 (unadjusted), reaction temperature = 30 °C). SEM images of (b, c) bare PVDF, (d, e) PBA-1@PVDF. Cycle test of PBA-1@PVDF: (f) absorption spectra of the SAM solution and (g) SAM degradation efficiency (reaction conditions: 5*10 cm^2 PBA-1@PVDF, $[PMS]_0 = 300$ mg/L, $[SAM]_0 = 10$ mg/L, pH 5.85 (unadjusted), reaction time = 60 min, reaction temperature = 30 °C). (h) XRD spectra of PVDF, PBA-1 and PBA-1@PVDF before and after repeated SAM degradation reactions.

$$SO_5^{\bullet-} + O^{2-} \rightarrow SO_4^{\bullet-} + O_2 \quad (8)$$

Depending on the concentration of the ROSs (*i.e.*, $SO_4^{\bullet-}$, $^{\bullet}OH$ and $^{\bullet}O_2^-$) present in the PBA-1/PMS system, SAM would be oxidized (Eq. 9). Additionally, the catalytic capability of PBA-1 depends on the excellent electron transfer and supports the face centered cubic structure. As a result, redox couple of the transition metals would cycle back and forth until complete consumption of PMS.

$$\text{ROSs} + \text{SAM} \rightarrow \cdots \rightarrow \text{Degradation products} \quad (9)$$

The excellent catalytic performance and stability of PBA-1 were proven. However, because of the poor recovery of the nanoparticles, the practical application of the as-obtained PBA-1 sample would be hindered. To improve the ability to separate the catalysts, the PBA-1 nanoparticles were assembled into a PBA-1@PVDF composite membrane. Then, the physicochemical property and catalytic capability of PBA-1@PVDF were measured and analyzed (as shown Text S6 in Supporting information).

As seen from Fig. 4a, the adsorption capability of the PBA-1 powders, PVDF and PBA-1@PVDF was determined, corresponding to the removal of 7.0%, 17.8% and 22.2% of SAM after 60 min, respectively. The superior adsorption performance of PBA-1@PVDF was ascribed to its tighter pore structure and smaller pore sizes, which were favorable to SAM adsorption. With addition of PMS, PBA-1 and PBA-1@PVDF exhibited an excellent catalytic capability, but PVDF achieved a SAM degradation efficiency of 20.8% after 60 min. These results indicated that PVDF had almost no catalytic ability when used as a base of the as-prepared composite membrane and mainly played roles in catalyst support and adsorption. Figs. 4b-e depicted the surface microstructure of the as-prepared PVDF and PBA-1@PVDF membranes. The PBA-1 nanoparticles that were doped into PVDF played a dominant role in activating the PMS process, so the PBA-1@PVDF/PMS reaction system achieved 71.7% degradation and 52.8% mineralization after 60 min (Fig. 4a and Fig. S13 in Supporting information). For comparation, the SAM degradation efficiency was 40.9% in PBA-1/PMS reaction system using a catalyst dosage of 20.0 mg/L. Therefore, with a relatively low mass ratio of catalyst (approximately 21.12 mg/L), the as-obtained composite membrane exhibited greater catalytic performance than PBA-1 nanoparticles. In addition, due to the even distribution of PBA-1 powder in the composite membrane, the agglomeration of nanoparticles was avoided. Meanwhile, PBA-1 is tightly wrapped in membrane matrix, so the physicochemical and catalytic properties of this membrane are more stable. As compared with the PBA-1/PMS reaction system, significant decreases in the Co and Fe leaching were observed in the PBA-1@PVDF/PMS system after a 60 min reaction. The Co leaching amount decreased from 0.259 mg/L to 0.018 mg/L, while the Fe leaching amount decreased from 0.128 mg/L to 0.002 mg/L.

More importantly, the reusability of the PBA-1@PVDF composite membrane was an important issue for its potential applications, and it was evaluated by performing ten consecutive reaction runs. As shown in Figs. 4f and g, the SAM degradation efficiency appeared to slightly decrease during the ten cycle experiments. Because SAM could not be directly mineralized in the degradation process, but would generate a variety of degradation intermediates, resulting in the deformation of the absorption spectra (Fig. 4f). Moreover, the XRD spectrum of PBA-1@PVDF after repeated catalytic reactions (Fig. 4h) also depicted the peak characteristic of PBAs, proving the existence and stability of PBA-1 in the composite membrane.

Overall, the abovementioned results confirmed that the PBA-1@PVDF membrane exhibited an excellent catalytic performance, a great separation and recovery ability, a much smaller demand of PBA-1, a slightly lower toxic metal ion leaching, and an adequate stability during the SAM degradation process. Therefore, PBA-1@PVDF could be used to oxidize organic contaminants.

In this work, CoFe PBAs were successfully synthesized *via* a facile co-precipitation treatment. Compared with other obtained PBAs, PBA-1 was shown to exhibit an excellent PMS activation capability for eliminating SAM (10 mg/L) in aqueous solutions, resulting in a slightly low EE/O value (0.01019 kWh/L) and metal leaching ($[Co] = 0.259$ mg/L, $[Fe] = 0.128$ mg/L). Furthermore, the influence of coexisting inorganic ions for various concentrations was

investigated. In fact, the PBA-1 particles possessed a special pore structure, an excellent stability and a tolerance to a wide pH range during the SAM oxidation. Additionally, PBA-1 addition produced $^{\bullet}OH$ and $SO_4^{\bullet-}$ and this was confirmed by the radical scavenging experiments and EPR. In addition, the reaction mechanism in the PBA-1/PMS system was proposed based on the results of XPS, and the decomposition pathways of SAM were proposed. Finally, we synthesized a PBA-1@PVDF composite membrane, which could be separated from reaction mixtures much more efficiently and expediently compared with the PBA-1 powder. More importantly, PBA-1@PVDF possessed good PMS activation capability and a great reusability, and thus, it could be considered for practical applications.

Declaration of competing interest

The authors declare that they have no known competing financial interests or personal relationships that could have appeared to influence the work reported in this pape

Acknowledgments

This work was kindly funded by National Natural Science Foundation of China (No. 51978319), Outstanding Youth Foundation of Gansu Province (No. 20JR10RA651), Natural Science Foundation of Xinjiang Uygur Autonomous Region (No. 2022D01C333), Science and Technology Project of Yili Kazak Autonomous Prefecture in 2022 (No. YZ2022Y003) and Research and Innovation Team Cultivation Program of Yili Normal University (No. CXZK2021004).

Supplementary materials

Supplementary material associated with this article can be found, in the online version, at doi:10.1016/j.cclet.2022.107837.

References

[1] C.M. Manaia, G. Macedo, D. Fatta-Kassinos, et al., Appl. Microbiol. Biotechnol. 100 (2016) 1543–1557.
[2] E. Sanganyado, W. Gwenzi, Sci. Total Environ. 669 (2019) 785–797.
[3] K. Schauss, A. Focks, H. Heuer, et al., TrAC Trends Anal. Chem. 28 (2009) 612–618.
[4] Y. Zhang, A.Z. Gu, M. He, et al., Environ. Sci. Technol. 51 (2017) 570–580.
[5] K. Zhang, Z.-G. Niu, Z. Lv, et al., Ecotoxicology 26 (2017) 1284–1292.
[6] W.-D. Oh, Z. Dong, G. Ronn, et al., J. Hazard. Mater. 325 (2017) 71–81.
[7] P. Westerhoff, Y. Yoon, S. Snyder, et al., Environ. Sci. Technol. 39 (2005) 6649-6663.
[8] S. Zhang, X. Peng, Z. Yue, et al., Chem. Eng. J. 397 (2020) 125466.
[9] R. Zhang, Y. Wan, J. Peng, et al., Chem. Eng. J. 372 (2019) 796–808.
[10] M. Ahmadi, F. Ghanbari, A. Alvarez, et al., Korean J. Chem. Eng. 34 (2017) 2154–2161.
[11] T. Olmez-Hanci, I. Arslan-Alaton, Chem. Eng. J. 224 (2013) 10–16.
[12] W.D. Oh, Z. Dong, T.T. Lim, Appl. Catal. B 194 (2016) 169–201.
[13] M. Sánchez-Polo, M.M. Abdel daiem, R. Ocampo-Pérez, et al., Sci. Total Environ. 463-464 (2013) 423–431.
[14] J. Wang, S. Wang, Chem. Eng. J. 334 (2018) 1502–1517.
[15] R. Guo, Y. Wang, J. Li, et al., Appl. Catal. B 278 (2020) 119297.
[16] M.B. Zakaria, T. Chikyow, Coord. Chem. Rev. 352 (2017) 328–345.
[17] S.S. Nadar, L. Vaidya, S. Maurya, et al., Coord. Chem. Rev. 396 (2019) 1–21.
[18] M. Cheng, C. Lai, Y. Liu, et al., Coord. Chem. Rev. 368 (2018) 80–92.
[19] L. Zeng, L. Xiao, X. Shi, et al., J. Colloid Interface Sci. 534 (2019) 586–594.
[20] S. Wu, G. Zhuang, J. Wei, et al., J. Mater. Chem. A 6 (2018) 18234–18241.
[21] W. Zhang, H. Zhang, X. Yan, et al., J. Hazard. Mater. 387 (2020) 121701.
[22] L. Clarizia, D. Russo, I. Di Somma, et al., Appl. Catal. B 209 (2017) 358–371.
[23] P.J.J. Alvarez, C.K. Chan, M. Elimelech, et al., Nat. Nano 13 (2018) 634–641.
[24] K.R. Zodrow, Q. Li, R.M. Buono, et al., Environ. Sci. Technol. 51 (2017) 10274–10281.
[25] J. Wang, S. Zhuang, Y. Liu, Coord. Chem. Rev. 374 (2018) 430–438.
[26] P. Kaner, E. Rubakh, D.H. Kim, et al., J. Membr. Sci. 533 (2017) 141–159.
[27] R. Guo, Y. Zhu, X. Cheng, et al., J. Hazard. Mater. 399 (2020) 122966.
[28] L. Lai, J. Yan, J. Li, et al., Chem. Eng. J. 343 (2018) 676–688.
[29] Y. Zhou, J. Jiang, Y. Gao, et al., Environ. Sci. Technol. 49 (2015) 12941-12950.
[30] F. Chen, G.X. Huang, F.B. Yao, et al., Water Res. 173 (2020) 115559.
[31] J.C. Crittenden, S. Hu, D.W. Hand, et al., Water Res. 33 (1999) 2315–2328.
[32] D. He, Y. Cheng, Y. Zeng, et al., Chemosphere 240 (2020) 124979.
[33] R. Xiang, Y. Duan, C. Tong, et al., Electrochim. Acta 302 (2019) 45–55.
[34] S. Devaramani, P.S. Adarakatti, P. Malingappa, Electrochim. Acta 231 (2017) 650–658.
[35] W.E. Buschmann, J.S. Miller, Inorg. Chem. 39 (2000) 2411–2421.
[36] J.A. Khan, X. He, N.S. Shah, et al., Chem. Eng. J. 252 (2014) 393–403.
[37] J. Li, Y. Ren, F. Ji, et al., Chem. Eng. J. 324 (2017) 63–73.
[38] K.Y.A. Lin, Z.Y. Zhang, Chem. Eng. J. 313 (2017) 1320–1327.
[39] X. Duan, Z. Ao, H. Zhang, et al., Appl. Catal. B 222 (2018) 176–181.
[40] M. Xu, J. Li, Y. Yan, et al., Chem. Eng. J. 369 (2019) 403–413.
[41] Y.D. Dong, L.Q. Zhang, P. Zhou, et al., J. Hazard. Mater. 423 (2022) 127054.
[42] R. Yin, W. Guo, H. Wang, et al., Chem. Eng. J. 335 (2018) 145–153.
[43] W. Qin, G. Fang, Y. Wang, et al., Chem. Eng. J. 348 (2018) 526–534.
[44] Y. Bao, W.D. Oh, T.T. Lim, et al., Water Res. 151 (2019) 64–74.
[45] Y. Liu, H. Guo, Y. Zhang, et al., Environ. Pollut. 252 (2019) 1042–1050.
[46] J. Chen, C. Fang, W. Xia, et al., Environ. Sci. Technol. 52 (2018) 1461-1470.
[47] F. Ghanbari, M. Moradi, Chem. Eng. J. 310 (2017) 41–62.
[48] B.T. Zhang, W. Xiang, X. Jiang, et al., J. Environ. Eng. 142 (2016) 04016003.
[49] F. Zheng, D. Zhu, X. Shi, et al., J. Mater. Chem. A 3 (2015) 2815–2824.
[50] S. Lei, Q.H. Li, Y. Kang, et al., Appl. Catal. B 245 (2019) 1–9.
[51] J. Zou, J. Ma, L. Chen, et al., Environ. Sci. Technol. 47 (2013) 11685-11691.
[52] M. Li, R. Luo, C. Wang, et al., Chem. Eng. J. 372 (2019) 774–784.
[53] H. Xu, D. Wang, J. Ma, et al., Appl. Catal. B 238 (2018) 557–567.
[54] H. Zhu, J.F. Zhang, R.P. Yanzhang, et al., Adv. Mater. 27 (2015) 4752–4759.
[55] E.L. Hu, Y.F. Feng, J.W. Nai, et al., Energy Environ. Sci. 11 (2018) 872–880.
[56] H. Lu, M. Sui, B. Yuan, et al., Chem. Eng. J. 357 (2019) 140–149.
[57] S. Lu, G. Wang, S. Chen, et al., J. Hazard. Mater. 353 (2018) 401–409.
[58] M.M. Kuklja, E.A. Kotomin, R. Merkle, et al., Phys. Chem. Chem. Phys. 15 (2013) 5443–5471.